

# TD-DFT investigations on structural modification in Carbazole based organic Photosensitizers to improve electron injection in DSSC

Abdul Majid<sup>1</sup>, Maryam Sana<sup>1</sup>, Salah Khan<sup>2</sup>, Zeyad Almutairi<sup>2</sup>, and Naeem Ahmad<sup>3</sup>

<sup>1</sup>University of Gujrat

<sup>2</sup>King Saud University

<sup>3</sup>International Islamic University

May 5, 2020

## Abstract

Time-dependent density functional theory approach implemented at hybrid-B3LYP, GGA-PBE and DFTB levels of theory was used to model photoinjection in organic-dye/TiO<sub>2</sub> quantum-dot to explore the prospects of improvement of DSSC. The photosensitizer used in this study consisted of six carbazole based organic dyes having acceptor as cyanoacrylic acid group and oligothiophene  $\pi$ -bridge spacer. The modifications were made in the dyes by increasing length of the spacer by adding thiophene and oxadiazole rings at different positions of the donor-acceptor bridge. The structural variations appeared to alter the electronic and optical properties of dyes studied via energy levels and excitation spectra. The UV-Vis spectra calculated for all the dyes in solvents exhibited a red shift in spectral peaks with increase in polarity of the solvents. The findings of the study pointed towards photoinjection of indirect nature studied in dye-(TiO<sub>2</sub>)<sub>96</sub> complex for six different dyes. The substitution of oxadiazole ring in center and addition of a thiophene ring at the edge of the spacer produced two dyes which exhibited lowest injection energies of 0.11eV and 0.17 eV along with the regeneration energies of 1.18 eV and 1.12 eV respectively. The dyes reported herein may have promising applications in photoanode for enhancing the performance of DSSC.

## 1. Introduction

The provision of sustainable, renewable, human friendly and cheap energy sources is demand of utmost priority for future living on earth. The available possibilities to obtain such sources principally points the scientific attention towards utilization of solar energy to meet up the energy requirements [1]. There has been several strategies and devices to harvest the solar energy out of which photovoltaic cells have been of prime research and industrial interest. A survey of last 15 years indicates that the first and second generation solar cells, offering respective efficiencies of 20% and 30%, have dominated the market with 30% manufacturing annual growth rate [2-5]. However, considering the simplest synthesis, mechanism and the basic requirements mentioned above, dye-sensitized solar cell (DSSC) is taken as most auspicious device among all generations of solar cells [6].

The conversion of solar energy to electric energy by DSSC takes place in two steps; first is generation of charge by photoactive specie as a result of absorption of incident photon of visible region and the second is transportation of charge by semiconductor and electrolyte. Despite of the low production cost, the reported efficiency of DSSC till date is 12% which is very low when compared with first and second generation solar-cells [7]. The issue of low efficiency, if could not be addressed, may limit the utilization of DSSC in future technology. The efficiency of DSSC relies heavily on photoanode which is basically dye-semiconductor complex. DSSC comprises of three major parts; semiconductor coated with photosensitizer (Dye), electrolyte and counter-electrode. The working mechanism of DSSC is sketched in figure1.

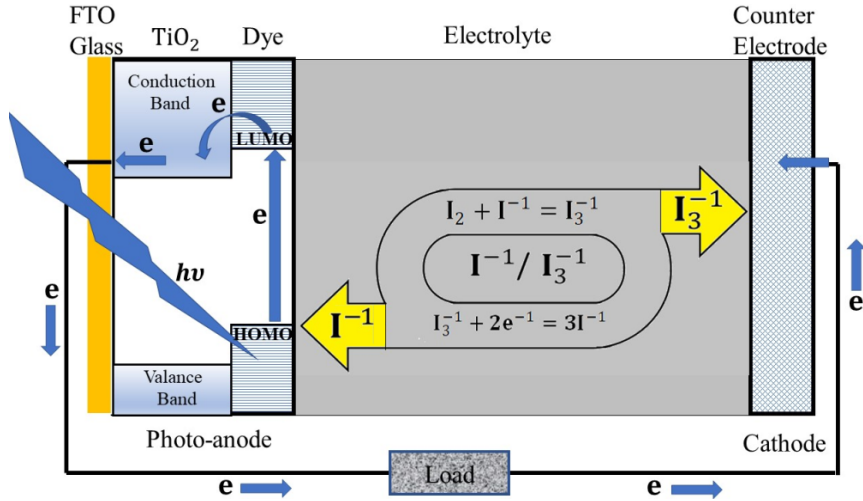


**Figure-1:** Working principle, mechanism and major components of a Dye Sensitized Solar Cell

Photosensitizer which play important role in operating cycle of DSSC may be metals-containing inorganic dyes or metals-free organic dyes. The community is inclined to build DSSC based on organic dyes due to high cost and environmental hazards of inorganic dyes [8, 9]. The organic dyes are environmentally friendly, low cost, having elevated extinction coefficient, affordable and available due to simple synthesis strategies. The photosensitizers having D- $\pi$ -A configuration are known to offer high efficiency [10]. In this configuration, Donor (D) must be an electron rich specie that donates electrons, acceptor (A) is electron deficient specie that accept electrons and these are connected by  $\pi$ -spacer whereas the acceptor is directly attached to surface of semiconductors (usually  $TiO_2$ ). The basic purposes of the dyes are absorption of light and transfer of charge which are strongly dependent on its structure and electronic properties [11]. There have been variety of donor groups such as phenothiazine [12, 13], Carbazole [14, 15], triphenylamine[16] and coumarin [17]. The efficient acceptors are alkoxysilane [18] and cyanoacrylic acid [19] whereas  $\pi$ -spacer could have units of different organic groups including dioxythiophene [20], benzene [21], benzothiadiazole [22] and thiophene [23]. The organic sensitizers based on triphenylamine are proven to offer elevated photoelectric conversion in DSSC because of its ability to restrict the dye aggregation and to facilitate the hole transferring [24].

There have been numerous attempts on tuning the properties of photosensitizers having different configuration [12-26]. The modifications in the configuration of the dyes thereby using different donors, acceptors and spacers appeared to change in their efficiencies. The  $\pi$ -bridge length of organic dyes greatly affects the molecular structure which causes the changes in band gaps, emission spectra and optoelectronic properties [25, 26]. The formation of different  $\pi$ -spacers is an effective strategy to increase the efficiency of the dyes due to its role in transferring the charge from donor to acceptor unit. This consideration predicts that a long chain of oligothiophene in  $\pi$ -spacer could give improved results. On the other hand,  $\pi$ - $\pi$  stacking in  $\pi$ -spacers of organic sensitizers typically occurs due to sturdy intermolecular interface. The  $\pi$ - $\pi$  pile is beneficial to light harvesting efficiency (LHE) due to its role in optoelectronic properties of the dyes that can be studied using UV-Visible excitation spectrum. Mostly the  $\pi$ -stacked accumulation results in incompetent electron injection that leads to inefficient light harvesting [27]. The proscription of  $\pi$ - $\pi$  heap taking place via preservatives in solution of dye is usual method to get better effectiveness of organic DSSC suffering from  $\pi$ - $\pi$  stacking trouble. The co-adsorption of additives along with dye [28] and structural alteration of sensitizers [29] have been found effective to avoid dye aggregation or  $\pi$ - $\pi$  stacking and therefore lead to improved efficiency of DSSC. The organic dyes with D- $\pi$ -A design are widely studied because of their efficient photosensitizing properties [30-32]. The hydrogen production and overall performance of DSSC is greatly affected by the length of  $\pi$ -spacer [33-38].

The process of photoinjection happening through photoanode is at heart of DSSC. The incident light is

absorbed by dyes to excite electrons from their HOMO to LUMO and the excited electrons are then injected to semiconductor. The dyes offering elevated oscillator strength are beneficial for photoinjection in photoanode of DSSC. The light harvesting ability of organic dyes can be tuned by suitable modifications which has been studied in this work. The injection of electron from dye to semiconductor could be done in two different ways; direct and indirect. The injection could be direct when electron move directly from HOMO of dye to conduction band (CB) of semiconductor which is characterized by occurrence of new peaks in spectrum. The indirect injection of electron involves shift of electron from the LUMO of excited dye moves toward the CB of semiconductor that is characterized by broadening of peaks in spectrum [39-41]. The adsorption of dyes on semiconductor is carried out by dissolving the dyes in suitable solvents. The process of solvation affects the optical properties of dyes [42, 43] due to which the choice of solvent should be made carefully. It has been often observed that dyes show red/blue shifts on solvation in different solvents [44].

This work involves computational investigations of carbazole based new organic dyes and study on their solvation effects to model the photoinjection for improvement in the current organic DSSCs. The dyes studied herein follows the molecular structure (3)D- $\pi$ -A in which the donor is oxidized by giving electrons through  $\pi$ -bridge to the acceptor. The carbazole are electron rich species which are known as organic photo-conductor(OPC) [45, 46] and act as donor in sensitizers creating photo-injected electrons having long life time by delaying the charge recombination at interfaces [47, 48]. Moreover carbazole is highly stable, starburst like twisted structure which allows efficient photo-sensitizing parameters[23, 49] and have high molar extinction coefficient [50].

## 2. Computational Details

The analytical solution to the problems related to structural modifications and modeling of photoinjection in organic dyes is a cumbersome task. Thanks to the development of different commercial codes and upgradation of computational infrastructures in recent past, the numerical solution to such problems with high reliability, precision and reproducibility are now possible. This work was carried out using LCAO (linear combination of atomic orbitals) based approach implemented in DFT code ADF (Amsterdam Density Functional) version 2018 which performs DFT, time dependent DFT (TD-DFT) [51] and Density-Functional based tight binding (DFTB) calculations [52] by computationally employing formulism of Kohn-Sham theory in fast and efficient way [53].

In order to investigate the effects of structural modification of carbazole-donor based organic dye on photoinjection, three dyes, named here as D1, D2 and D3 , shown in figure 2, were used as reference [23]. The length of the  $\pi$ -spacer of carbazole-donor based organic dye with oligothiophene  $\pi$ -spacer having carboxylic acid as acceptor was increased by adding thiophene units.

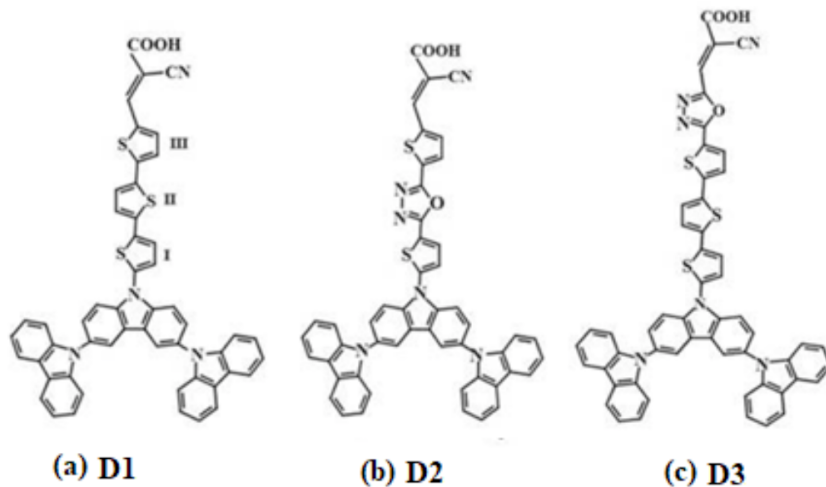


**Figure-02:** Carbazole-Donor Based Organic Dyes (a) Dye-1(D1); (b) Dye-2(D2); (c) Dye-3(D3) [23]

In order to get structure of D1, carbazole dendritic was attached with thiophene bridge comprising of 3 thiophene rings connected with each other via carbon atoms. The carbazole dendritic was attached to thiophene bridge at 125° in order to get non-planer structures where the third thiophene ring was connected with carbon of cyanoacrylic acid. D1A is modified form of D1 which was obtained by adding a thiophene ring at 4<sup>th</sup> position of thiophene bridge.

The structure of D2 is derived from D1, it contains carbazole dendritic as donor and cyanoacrylic acid as acceptor, with the difference of π-spacer in such a way that D2 contains an oxadiazole ring substituted in place of 2<sup>nd</sup> thiophene ring. D2A is modified form of D2 which was obtained by adding a thiophene ring at 4<sup>th</sup> position in π-spacer.

The structure of D3 is derived from D1 by adding an oxadiazole ring at 4<sup>th</sup> position of thiophene bridge of π-spacer. D3A is modified form of D3 which was obtained by adding an extra thiophene ring at 4<sup>th</sup> position and oxadiazole at 5<sup>th</sup> position in the π-spacer.

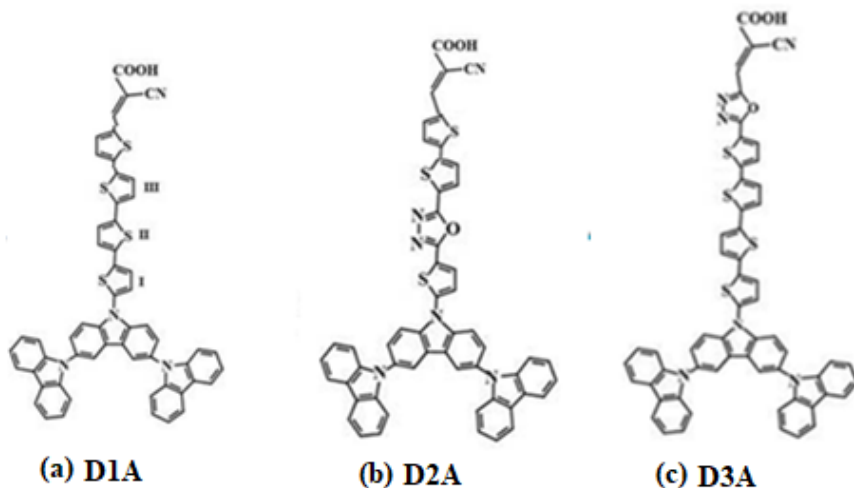


**Figure-03:** Carbazole-Donor Based Modified Organic Dyes: (a) D1A (b) D2A (c)D3A

The molecular structures of dyes comprise of 91 atoms in D1, 89 atoms in D2, 96 atoms in D3, 98 atoms in D1A, 96 atoms in D2A and 103 atoms in D3A. The Slater type basis and fit functions were used with number of 4 for H, 9 for C, 9 for N, 13 for S, 9 for O. The entire calculations were done without enforcing any symmetry. The structures were pre-optimized using universal force field and then geometries were optimized to ensure complete relaxation of the molecules/structures at minimum possible energy. In the course of structural relaxation, the geometry updates involved ‘delocalized’ optimization coordinates with BFGS (Broyden-Fletcher-Goldfarb-Shanno) as Hessian update algorithm.

The basis functions were in the form of Slater Type Orbitals (STOs) of quality TZP (core double zeta, valence triple zeta, single polarized basis set) for all atoms used in the dye molecules. The exchange and correlation functional (XC) was separately taken as standard GGA-PBE and hybrid BLYP for all cases studied in this work. The iterative geometry improvements involved convergence criteria with changes in energy, gradients and bond length changes as 0.02 eV, 0.02 eV/Å and 0.01 Å whereas the SCF updates of geometry were carried out with convergence criterion of  $2.7 \times 10^{-5}$  eV. The numerical integrations were carried out with Becke grid quality and ZlmFit density fit Quality as ‘Good’. The precision parameters involved in numerical integration was 6.0000000000 whereas the basis and fit neglect functions were  $0.1 \times 10^{-7}$ . The linear scaling parameters of cut-off radii density fit, overlap cut-off criterion for Coulomb potential and multipole terms were  $0.1 \times 10^{-9}$ ,  $0.1 \times 10^{-7}$ ,  $0.1 \times 10^{-9}$  and  $0.1 \times 10^{-9}$  respectively. The entire calculations were of all-electron type in such a way that no of core orbitals were considered for finding the orbital energies. The ADF calculates the value of bond energy by finding the difference of energy between molecule and its fragments in the form of spherically symmetric and spin restricted atoms [54].

$(\text{TiO}_2)_{96}$  quantum dot having 96 atoms of Ti and 192 atoms of O was prepared using DFTB by employing SCC-DFTB model. The dispersion and periodicity were set as ‘none’ and the parameter set trio/org 0-1 was used thereby setting Fermi temperature at 5 K. The default values of occupation and initial hessian were selected. The energy convergence, gradient convergence and step convergence are  $10^{-5}$  eV,  $10^{-3}$  eV/Å and  $10^{-3}$  respectively. The optimization method and optimization space were employed as quasi-newton method and cartesian space respectively.

After the geometry optimization of the structures, all electrons single point calculations were done, on the optimized neutral dye structures without considering symmetry, in order to study electronic and optical characteristics of photosensitizers. The UV-Vis excitation spectrum was calculated using ADF-Response code by considering the singlet-singlet allowed transitions by utilizing Davidson method [55]. The properties of the structures optimized at corresponding levels of theory were calculated using XC functionals GGA-PBE and Hybrid-B3LYP. The criterion of convergence was adopted as  $10^{-6}$  eV thereby setting the numerical quality ‘good’ with basis set TZP. The excitation spectra were also calculated using DFTB with model SCC-DFTB by selecting singlet-singlet transitions with both Davidson and exact methods.

In order to study the photoinjection, the already optimized dye molecules were adsorbed on the surface of optimized  $(\text{TiO}_2)_{96}$  quantum dot (QD) by performing geometry optimization at DFTB level of theory using Canonical DFTB algorithm. A complete SCC convergence was ensured with gradient convergence of 0.01 Hartree/Å and charge convergence of  $10^{-8}$  e at Fermi temperature of 300 K. The atoms of the QD were kept fixed except the unit involved in binding with dye acceptor. Further, the entire atoms of the dyes were allowed to relax during the optimization of QD-Dye complex. The excitation spectra on the optimized QD-Dye complexes were calculated in single point runs to study the photoinjection by employing the stated parameters. The electron occupation in shells and sub shells are set as ‘default’ that include both fermi and aufbau principal and with K-space sampling as ‘gamma’. Transition charges in these calculations are pre-calculated. From excitation spectra, photoinjection energy, recombination energy and LHE were calculated.

The effects of solvation were also studied by optimizing the dyes structure in two solvents; water and methanol. The number of molecules of solvents and the polarity of solvents are important factors that should be kept in mind during these calculations. The parameters that are used in geometry optimization of dyes and dyes-TiO<sub>2</sub> were also utilized for relaxation of dyes in solvents. The solvent radius was set as 10.0 where the solute factor was set as 2.7 that comprise almost 27 solvent molecules relative to one molecule of dye.

As the dyes get relaxed in solvents then their UV-Vis excitation spectrums of all the dyes were calculated in order to study the spectral shift in dyes due to solvation.

### 3. Results and Discussion:

The fully relaxed structures of six photosensitizer dyes were attained at different levels of theory hybrid-B3LYP, GGA-PBE and SCC-DFTB. The excitation spectra and photoinjection in dye-(TiO<sub>2</sub>)<sub>96</sub> system for all dyes was studied in vacuum and solvents for improving the performance of DSSC. The results on excitation spectra and optical transitions in D1, D2 and D3 have been reported elsewhere [20]. However, the description involving these dyes is given here for sake of completeness with addition of photoinjection as well as solvation effects involving these three dyes. The magnitude of molecular dipole moment, calculated with analytic integration using PBE were 1.680 for D1, 2.195 D2, 2.246 for D3, 2.001 for D1A, 2.027 for D2A and 1.769 for D3A. In what follows, the calculated results and discussion to shed light on photoinjection in all 6 dyes are described.

#### 3.1. Structural Properties

The dyes studied in this work are of (3)D- $\pi$ -A type, where donor mentioned as D is electron rich specie, the acceptor mentioned as A is electron deficient specie and spacer connecting them is in form of  $\pi$ -bridge. The dyes D1 and D1A contain carbazole dendritic as oxidizing donor specie, cyanoacrylic acid as accepter reduction species connected via variable length  $\pi$ -bridge of thiophene rings. In D1, there are 3 carbazole donors with each comprising of three rings in which 2 rings are 6-membered benzene ring attached from both side to nitrogen containing 5-member ring. The 1<sup>st</sup> and 2<sup>nd</sup> carbazole members are attached to 3<sup>rd</sup> carbazole member via their nitrogen atoms. The Donor are then attached to  $\pi$ -bridge consisting of three oligothiophene units named as I, II and III as shown in figures 2 and 3. The  $\pi$ -bridge acts as a charge transfer channel which receives electrons from the donorto pass on to the acceptor specie which finally transports it to the semiconductor. Oligothiophene have property of self-assembly and it enhances the transfer of charge from donor to acceptor.

D1A have similar structure as D1 will an additional oligothiophene unit at IV position as shown in figure 3. The respective values of length of  $\pi$ -spacer in D1 and D1A after optimization are 10.32 and 14.23 whereas angle between the donor and  $\pi$ -spacer is 125.7° for both the dyes.

The D2 contains an oxadiazole ring between two thiophene rings. The addition of electrophilic heterocyclic molecules with thiophene in  $\pi$ -spacer can produce such changes in energy levels which are favorable for photosensitizers [55-57]. Oxadiazole is an efficient electron acceptor with elevated thermal stability and photoluminescence quantum yield [58]. The oxadiazole has high compatibility with thiophene because of their structural similarities [59]. Hence, the efficient electron accepting ability of oxadiazole and its compatibility with thiophene can lead to tune the properties of molecules base on thiophene. The structure of D2A is similar as D2 except an extra thiophene ring at IV position in the  $\pi$ -spacer. The respective values of length of  $\pi$ -spacer in optimized structures of D2 and D2A are 9.75 and 13.6 whereas there is an angle of 125° between donor and  $\pi$ -spacer for both the dyes.

The D3 contains an oxadiazole ring at 4<sup>th</sup> position of thiophene bridge of D1 whereas D3A has an additional oxadiazole at V position in  $\pi$ -spacer. The values of length of  $\pi$ -spacer in optimized structures of D3 and D3A are 10.2, 17.4 whereas there is an angle of 125° between donor and  $\pi$ -spacer for both dyes.

#### 3.2. Optical/Electronic Properties of Dyes

The increase in the length of  $\pi$ -spacer is expected to enhance the oscillator strength and lessen the excitation energy to induce transitions. A detailed analysis of energy levels, especially HOMO and LUMO, is made to understand the effects of structural modification on optical and electronic properties of the dyes. The (TiO<sub>2</sub>)<sub>96</sub> was optimized with mean diameter as 2.7 nm whereas the calculated value of HOMO-LUMO gap was 1.9 eV.

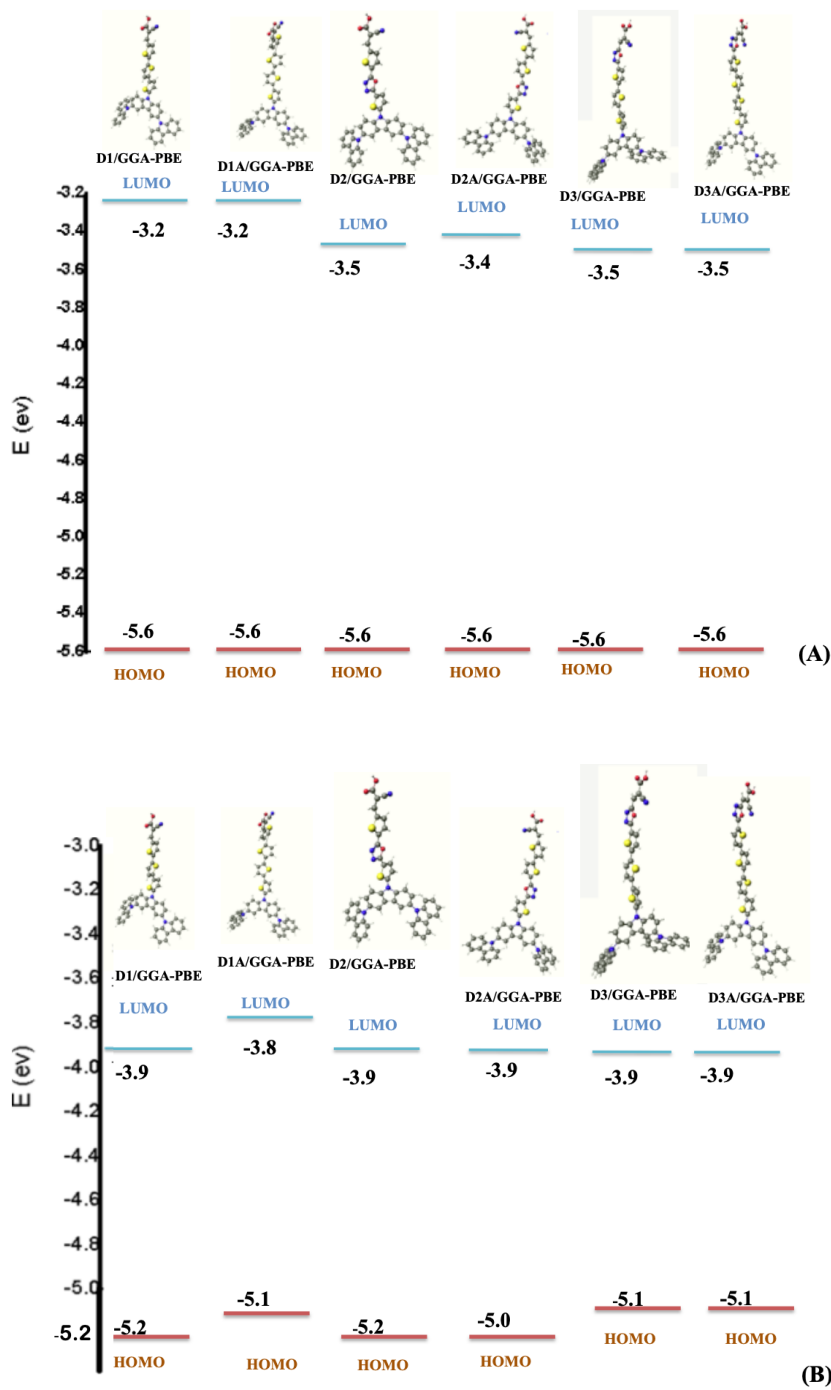
The HOMO and the LUMO energy levels of dye for a competent injection of electron should be compatible

with the semiconductor. The LUMO of the dyes should be more negative than the CB of semiconductor (frequently used  $\text{TiO}_2$ ) [60,61] and energy of HOMO ought to be lower than the oxidation and reduction potential of electrolyte (frequently  $\text{I}^{-1}/\text{I}^{-3}$  redox couple is utilized) [62]. Moreover, a small band gap is preferred to excite electron from HOMO of dye to its LUMO in order to make the transition by providing the small amount of energy. Table 1 clearly shows that the LUMO of all the dyes simulated in this work is more negative than the CB of the QD. In addition to this the HOMO of these dyes are less negative than the redox potential of electrolyte, which results in competent renewal of dyes.

The energy of HOMO level of both dyes D1 and D1A is found less than HOMO of redox electrolyte  $\text{I}_3^-$  (-4.8eV) that results in effective regeneration of dye whereas the energy of LUMO of both dyes is greater than energy of LUMO of  $\text{TiO}_2$  (-4.3 eV) which may cause easy injection of electron from dye to  $\text{TiO}_2$ . The energies of LUMO and HOMO of D1 and D1A, obtained by utilizing ADF/TD-DFT with the XC functional set as GGA-PBE Hybrid- B3LYP and SCC-DFTB. The respective values of HOMO of D1 is at -5.0 eV, -5.6eV [23], 5.2 eV and LUMO at -3.9 eV, -3.2 eV [23] and -3.9 eV with band gap -1.1 eV, -2.4 eV and -1.3 eV calculated using GGA-PBE, Hybrid-B3LYP and SCC-DFTB. In case of D1A, the respective values of HOMO and LUMO are -4.9 eV, -5.6 eV, -5.1 eV and -3.8eV, -3.2eV, -3.8 eV with same band gap as that of D1 calculated for all three functionals. The comparison indicates that the energy of HOMO increases from D1to D1A which shows a clear increase in the energy of HOMO level with increase in length of  $\pi$ -bridge in agreement with literature [63]. Likewise, the changes in energy of LUMO level are noted but very negligible change in case of Hybrid-B3LYP are observed for both HOMO and LUMO [63-65].

The HOMO of D2 is found at -5.0 eV, -5.6 eV [23], -5.2 eV and LUMO at -4.1 eV, -3.5eV [23], -3.9 eV with band gap of 0.9 eV, -2.1 eV and -1.3 eV calculated using-PBE, Hybrid-B3LYP and SCC-DFTB respectively. On the other hand, the HOMO of D2A is found at -5.0 eV, -5.6 eV, -5.2 eV and LUMO level is at -4.0 eV, -3.4 eV, -3.9 eV with a band gap of 1.0 eV, -2.2 eV, -1.3 eV calculated for three respective functionals. The addition of electron withdrawing group oxadiazole in  $\pi$ -bridge has led to change in LUMO energy level because of change in charge transfer, while the energy of HOMO remains same as the values of band gaps for D1 are larger than D2. The decrease in value of band gap of D2 upon addition of electron withdrawing oxadiazole group is due to lowering of its LUMO level [64]. A slight increase in band gap has taken place when  $\pi$ -bridge length was increased for D2A.

The HOMO of D3 is found at -5.0 eV, 5.6 eV [64], -5.1 eV and LUMO is at -4.2 eV, 3.5 eV [64], -3.9 eV with a band gap of 0.8 eV, -2.1 eV and -1.2 eV when calculated using the respective functionals. On the other hand, in case of D3A the HOMO level is found at -5.0 eV, -5.6 eV, -5.1 eV and LUMO level is at -4.1 eV, -3.5 eV, -3.9 eV with a band gap of 0.9 eV, -2.1 eV and -1.3 eV when calculated using GGA-PBE, Hybrid-B3LYP and SCC-DFTB respectively. A decrease in value of band gap is observed on addition of electron withdrawing oxadiazole in D3 whereas a slight increase in band gap occurs when  $\pi$ -bridge length increases for D3A[64]. The comparative analysis of calculated values of HOMO, LUMO and their gap calculated using three functionals is sketched in figure 4.



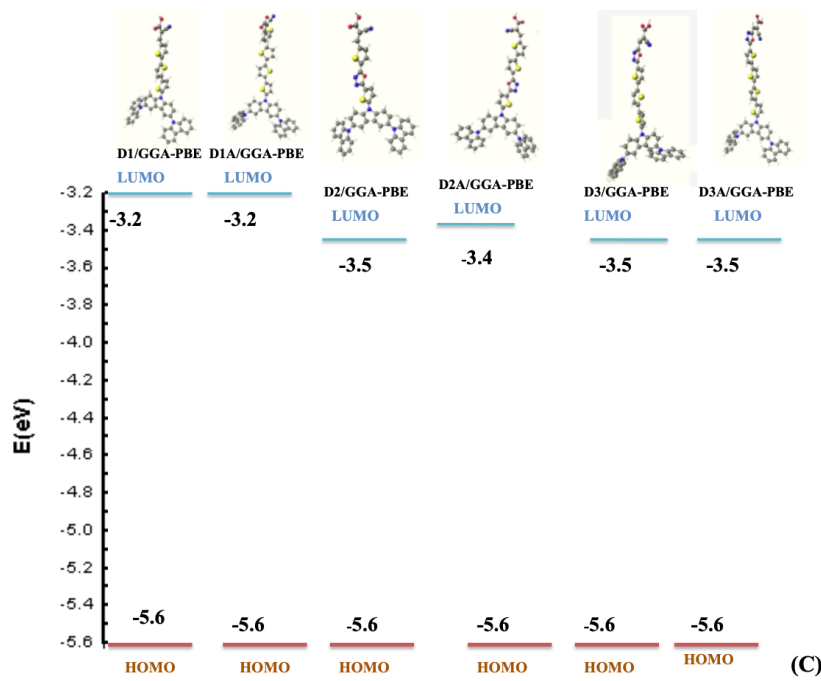


**Figure 4:** HOMO and LUMO energy levels calculated under TD-DFT study for D1, D1A, D2, D2A, D3 and D3A using (A) GGA-PBE, (B) SCC-DFTB and (C) Hybrid B3LYP

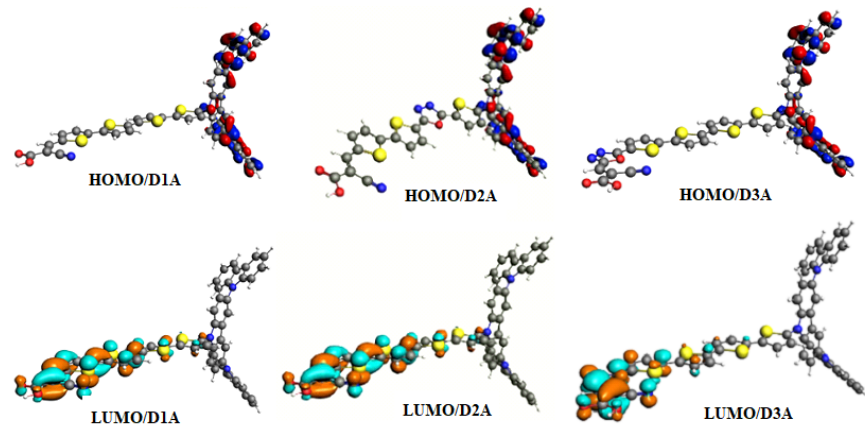


**Figure 5:** Images of HOMO and LUMO of D1A, D2A, and D3A found using Hybrid B3LYP

The energy values calculated for HOMO, LUMO and their gap calculated using three functionals employed in this study are listed in table 1.

Table- 1: Elec- tronic prop- erties of D1, D1A, D2, D2A,D3 and D3A by using GGA- PBE, DFTB and Hybrid- B3LYP/ DFT								
Dyes	GGA- PBE HOMO level (eV)	GGA- PBE LUMO Level (eV)	GGA- PBE Band gap (eV)	SCC- DFTB HOMO level(eV)	SCC- DFTB LUMO Level(eV)	SCC- DFTB Band gap(eV)	Hybrid- B3LYP HOMO Level(eV)	Hybrid- B3LYP LUMO gap(eV)
D1	-5.0	-3.9	1.1	-5.2	-3.9	1.3	-5.6	-3.2
D1A	-4.9	-3.8	1.1	-5.1	-3.8	1.3	-5.6	-3.2
D2	-5.0	-4.1	0.9	-5.2	-3.9	1.3	-5.6	-3.5
D2A	-5.0	-4.0	1.0	-5.2	-3.9	1.3	-5.6	-3.4
D3	-5.0	-4.2	0.8	-5.1	-3.9	1.2	-5.6	-3.5
D3A	-5.0	-4.1	0.9	-5.1	-3.9	1.2	-5.6	-3.5

### 3.3. Absorption spectra of Dyes

The allowed transitions of singlet-singlet nature were calculated using TD-DFT for D1, D1A, D2, D2A, D3 and D3A via UV-Vis spectra at GGA-PBE, SCC-DFTB and Hybrid-B3LYP levels of theory, as shown in figure 5. In case of GGA-PBE, the main absorption peak of D1 is found at 539 nm (2.3 eV) with oscillator strength of 1.01 and small absorption peak is found at 6391 nm with very small oscillator strength of 0.1. For D1A the main absorption peak is at 639 nm (1.94 eV) with oscillator strength 1.08 and a peak is found at 539 nm with oscillator strength 0.7. For SCC-DFTB calculations, the main absorption peaks for D1 and D1A are found at 652 nm (1.9 eV), 516 nm (2.4 eV), 688 nm (1.8 eV) and 590 nm (2.1 eV) having oscillator strengths of 0.68, 0.44, 0.68 and 0.46 respectively. In case of Hybrid-B3LYP, the absorption peaks are found at 495 nm (2.5 eV) and 539 nm (2.3 eV), 619 nm (2.0 eV) having oscillator strengths 0.95, 0.98 and 0.51 respectively for D1 and D1A. The spectra shows a red shift and broadening of peaks with increase in oscillator strength when  $\pi$ -spacer length has increased for D1A in agreement with literature [59, 61-65]. The main absorption peak for D2 is found at 688 nm (1.8 eV) with oscillator strength 0.16 using GGA-PBE whereas two absorption peaks are found at 619 nm (2.0 eV) and 495 nm (2.59 eV) with oscillator strength 0.38 and 0.66 respectively using SCC-DFTB. For D2A, there are two main absorption peaks at 688 nm and 563 nm with oscillator strength 0.27 and 0.24 in case of GGA-PBE where as there are three absorption peaks at 688 nm (1.8 eV), 619 nm (2.0 eV) and 539 nm (2.3 eV) having oscillator strengths 0.67, 0.45 and 0.67 respectively for SCC-DFTB. In case of Hybrid-B3LYP functional, the absorption peaks are found at 413 nm

(3.0 eV), 479 nm (2.6 eV) and 476 nm (2.6 eV) with oscillator strengths 0.90, 0.59 and 0.96 respectively for D2 and D2A. The oscillator strength has increased with increase in  $\pi$ -bridge length with small red shifts [63, 65-69].

There exist two absorption peaks for D3 at 774 nm (1.6 eV) and 688 nm (1.8 eV) with oscillator strength of 0.29 and 0.20 respectively. In case of D3A there is only one main absorption peak at 885 nm (1.4 eV) having oscillator strength of 0.45 with GGA-PBE. However, in case of SCC-DFTB, the absorption peaks are found at 688 nm (1.8 eV), 563nm (2.2 eV), 744 nm (1.6 eV), 619 nm (2.0 eV) with excitation respective values of oscillator strength as 0.53, 0.81 and 0.77,0.87 for D3 and D3A. Similarly, for Hybrid-B3LYP absorption peaks are found at 563 nm (2.2 eV), 413 nm (3.0 eV) and 476 nm (2.0 eV) with respective values of oscillator strength as 0.86, 0.90 and 0.85 for D3 and D3A. This is evident from the result that a red shift occurs and oscillator strength also enhanced in absorption spectrum when an length of  $\pi$ -bridge was increased for D3A [65-69].

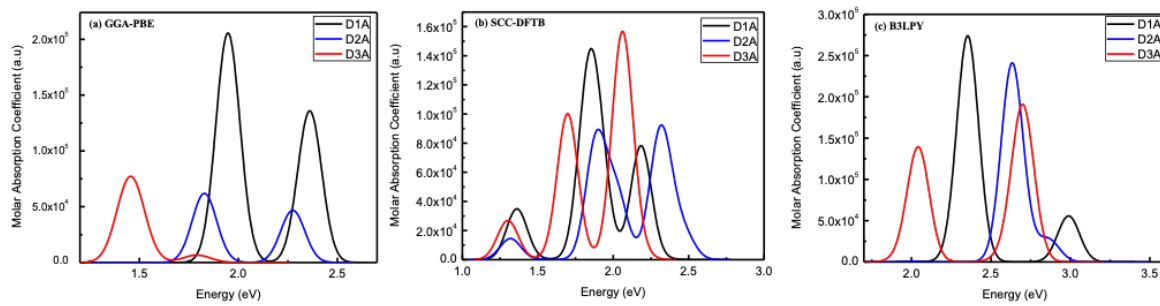


**Figure-5:** TD-DFT calculated UV-Vis spectrum of D1, D1A, D2, D2A, D3 and D3A from using (a) GGA-PBE (b) SCC-DFTB and (c) Hybrid-B3LYPfunctional



















### 3.4. Solvation affects

The emission and absorption characteristics of organic molecules are known to change by the process of solvation. The frequency, shape and intensity of peaks in the spectrum of fluorescent molecules changes when environment of the molecules changes from gaseous to liquid phase upon using solvents of different polarity [42, 70-75]. The properties of solvents and their interaction with solute molecules are responsible for the changes in electronic and optical properties of the molecules. Abundant studies are available on the relationship of solvent parameters and optical properties of photo-active solute molecules [42, 43, 76]. Different optoelectronic parameters as polarizabilities, refractive indices and electronic permittivity can be calculated by using different strategies developed on the basis of solvent action. Bakhshiev theory [42] is one of these methods to calculate the shift in spectrum upon the solvation by using the following relations;

$$v = u - u \quad (1)$$

$$u_{\max} = u_{\max,} + C_1 f(\varepsilon) + C_2 f(n) \quad (2)$$

Where  $u_{\max}$  is maximum wavenumber in solvent and  $u_{\max,}$  is maximum wavenumber in gaseous state and  $f(n), f(\varepsilon)$  are solvent factors depending on refractive index and electronic permittivity, respectively. The solute-solvent interaction can be effectively studied by solvatochromatic effect which is defined as the shift in spectrum (Stokes shifts) that usually depends upon relationship between polarity of solvent and emission spectrum of photoactive specie [77,78].

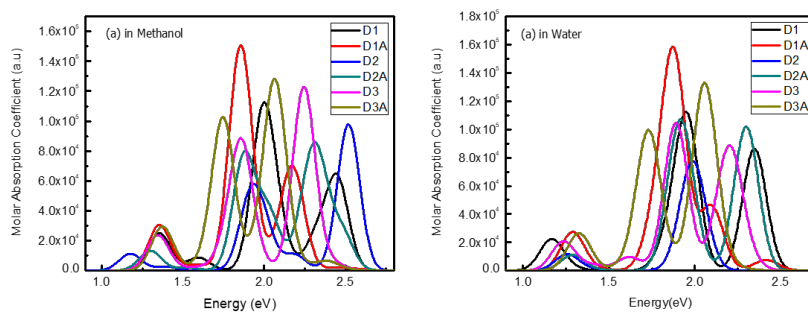


**Figure-6:** TD-DFT calculated UV-Vis spectra of D1, D1A, D2, D2A, D3 and D3A (a) in Methanol and (b) in Water by using SCC-DFTB

In order to get the understanding of the behavior of dyes in different solvents of varied polarity, the absorption spectrum of all dye were studied in methanol and water using TD-DFT at SCC-DFTB level of theory by utilizing parameters set org/tiorg-0-1 and solute factor of 2.7. The UV-Vis spectra calculated for all the dyes in methanol and water solvents is given in figure 6. The analysis exhibited a red shift in spectral peaks as the polarity of solvent is increased which depends upon properties of solvents and hydrogen bonding between solvent-solute and solute-solute molecules [42, 79, 80]. The amount of solvent has also affected the oscillator strength in addition to excitation energy of the photoactive species.

### 3.5. Photoinjection in TiO<sub>2</sub>-Dye Complex

As the light shines on the surface of dye, the electron from the HOMO of dye are excite to its LUMO after which the electron is moved to the conduction band of semiconductor TiO<sub>2</sub> [80]. This transfer of electron could be of two types: direct photoinjection and indirect photoinjection. The indirect transfer

involves transition HOMO-dye to LUMO-dye to CB-TiO<sub>2</sub> whereas the direct transfer comprises of transition HOMO-dye to CB-TiO<sub>2</sub>. These two processes are sketched in figure 7.

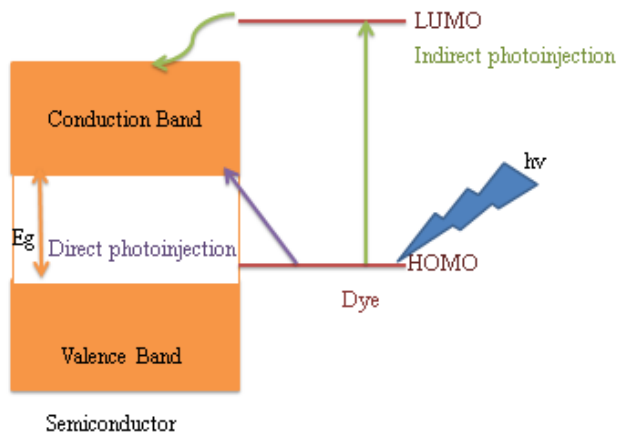


**Figure 7:** The schematic of charge transfer from dye to Semiconductor TiO<sub>2</sub>

The direct photojunction is usually indicated by appearance of an additional peak in excitation spectrum where no additional peaks are observed in indirect photojunction [39, 40, 81-83]. In this work a (TiO<sub>2</sub>)<sub>96</sub>QD having 288 atom and size 2.7 nm is utilized to model the photojunction in (TiO<sub>2</sub>)<sub>96</sub>-D complex where D = D1, D1A, D2, D2A, D3 and D3A. In order to prepare the series of complexes, the dyes were adsorbed on the surface of (TiO<sub>2</sub>)<sub>96</sub> in dissociative monodentate mode in which OH and O of the anchoring group were attached with respective oxygen and titanium atoms on surface of (TiO<sub>2</sub>)<sub>96</sub>[39, 84]. SCC-DFTB approach was utilized in order to get optimized geometries of dye-(TiO<sub>2</sub>)<sub>96</sub> complex with parameters utilized in these simulations are org/trio 0-1. The relaxed geometries of the complex were obtained by allowing the dye and its anchoring TiO<sub>2</sub> units to take part in geometry optimization whereas the rest of TiO<sub>2</sub> units were kept fixed in order to lessen the computational cost. UV-Vis excitation spectra were then obtained for the optimized complex at SCC-DFTB level of theory in order to model the photojunction in the mentioned complexes. The spectra obtained for all six complexes show small red shift and broadening of peaks in comparison to the bare dyes. The behavior of all dyes is changed after absorption on (TiO<sub>2</sub>)<sub>96</sub> whereas the extent of red shift in the adsorbed dyes is also different. The values of red shift for D1 and D1A are 0.26 eV and 0.21 eV respectively. D2 exhibited largest red shift of 0.85 eV whereas D2A, D3 and D3A show red shift of 0.14 eV, 0.04 eV and 0.1 eV respectively. The spectra of the adsorbed dyes shows a red shift that attribute to hybridization of orbits in density orbit stabilization [84]. This behavior points to the indirect photojunction in these dyes. The excitation spectra of bare dyes and dyes attached to TiO<sub>2</sub>QD are given in figure 8.

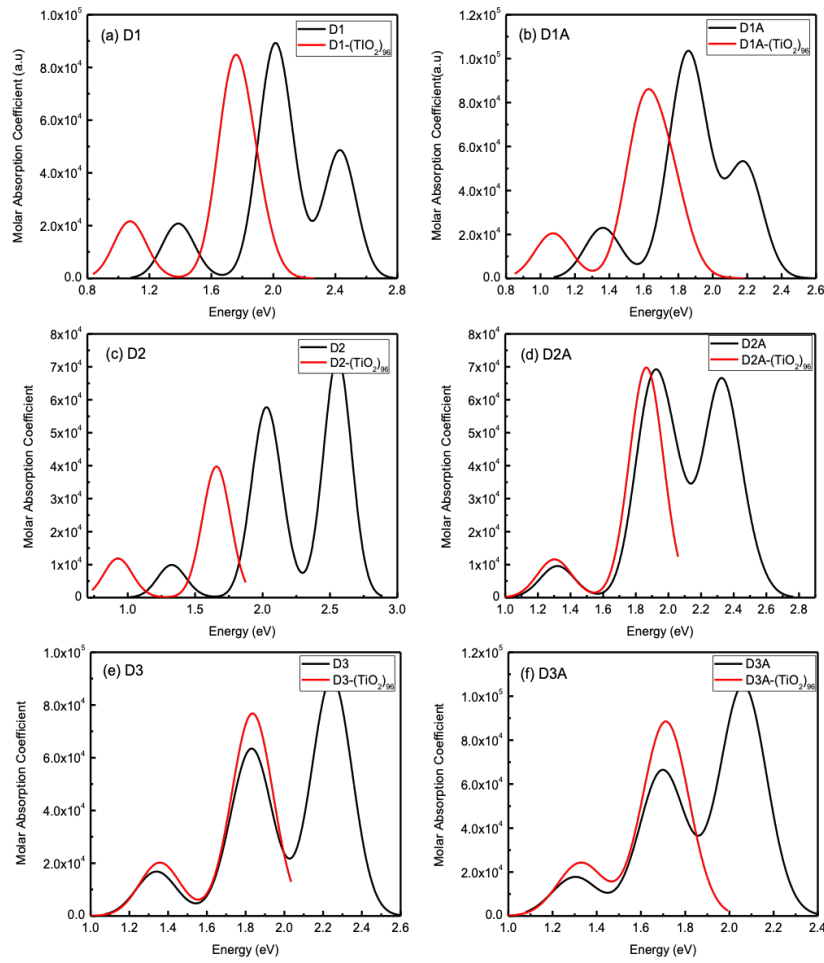


Figure-8: SCC-DFTB calculated excitation spectra for bare dyes and the dyes adsorbed on (TiO<sub>2</sub>)<sub>96</sub> QD in the form of QD-D system whereas D = D1, D1A, D2, D2A, D3 and D3A.

In order to model the mechanism and determine the driving force for photoinduction, the relevant parameters were calculated for the series of dye-(TiO<sub>2</sub>)<sub>96</sub> complexes. The energy required for photoinduction is [?]G<sub>inj</sub>(eV)= E<sub>LUMO</sub>-E<sub>CBM</sub> whereas the energy of electron recombination is [?]G<sub>rec</sub>(eV)= E<sub>CBM</sub>-E<sub>HOMO</sub>. The findings indicated that D2-(TiO<sub>2</sub>)<sub>96</sub> system required minimum energy of -0.11 eV for electron injection with high recombination energy of 1.18 eV which reveals that electron injection is more favorable than electron recombination. The complex D2A-(TiO<sub>2</sub>)<sub>96</sub> requires -0.17 eV for electron injection as second minimum value which is less than the recently reported carbazole based organic dyes [85]. The values calculated for all dye-(TiO<sub>2</sub>)<sub>96</sub> complexes are given in table 3.

| <b>Table-3:</b><br>Photoinjec-<br>tion<br>parameters<br>calculated<br>for $(\text{TiO}_2)_{96}\text{QD}$ -<br>Dcomplexes(D<br>= D1, D1A,<br>D2, D2A,<br>D3 and<br>D3A) |
|--|--|--|--|--|--|--|
| <b>System</b><br>$\text{D1-}(\text{TiO}_2)$  | <b>VBM (eV)</b><br>-6.07   | <b>HOMO (eV)</b><br>-5.22  | <b>CBM (eV)</b><br>-4.1  | <b>LUMO (eV)</b><br>-3.91  | <b>[?]G<sub>inj</sub> (eV)</b><br>-0.19  | <b>[?]G<sub>rec</sub> (eV)</b><br>1.12   |
| $\text{D1A-}(\text{TiO}_2)$  | -6.07  | -5.14  | -4.1   | -3.85  | -0.25  | 1.04   |
| $\text{D2-}(\text{TiO}_2)$   | -6.07  | -5.28  | -4.1   | -3.99  | -0.11  | 1.18   |
| $\text{D2A-}(\text{TiO}_2)$  | -6.07  | -5.22  | -4.1   | -3.93  | -0.17  | 1.12   |
| $\text{D3-}(\text{TiO}_2)$   | -6.07  | -5.19  | -4.1   | -3.90  | -0.20  | 1.09   |
| $\text{D3A-}(\text{TiO}_2)$  | -6.07  | -5.14  | -4.1   | -3.89  | -0.21  | 1.04   |
| 96   |  |  |  |  |  |  |

#### 4. Conclusions

A group of carbazole based organic dyes was simulated by increasing the  $\pi$ - bridge length by adding an additional oligothiophene ring in 3 different dyes. The increase  $\pi$ - bridge length significantly altered the optical and electronic properties of dyes. The addition of an extra oligothiophene ring resulted in increase of light harvesting efficiency whereas the absorption spectrum of the dyes exhibited redshift. Except the D3A, all the dyes exhibited absorption in visible region of light. The photoinjection of these dyes was studied by attaching the dyes with  $(\text{TiO}_2)_{96}\text{QD}$  in monodentate mode. The spectra calculated for  $(\text{TiO}_2)_{96}$ -Dye complexes indicated absence of any new peak which points to indirect photoinjection in the studied configurations. The findings indicated that D2 offered least electron injection energy -0.11 eV and least recombination rate due to high recombination energy calculated among all the dyes. After D2, D2A exhibited less injection energy of -0.17 eV. These dyes could have promising applications in photoanode for enhancing the efficiency of DSSC.

**5. Funding Information** The author would like to sincerely appreciate the Deanship of Scientific Research at King Saud University for its funding of this research through research group no. RGP-255.

#### 6. References

1. Grätzel, M., *Photoelectrochemical cells*. nature, 2001. **414** (6861): p. 338.
2. Zhang, Q. and G. Cao, *Nanostructured photoelectrodes for dye-sensitized solar cells*. Nano Today, 2011. **6** (1): p. 91-109.
3. Hagfeldt, A., et al., *Dye-sensitized solar cells*. Chemical reviews, 2010. **110** (11): p. 6595-6663.
4. Wenham, S. and M. Green, *Silicon solar cells*. Progress in Photovoltaics: Research and Applications, 1996. **4** (1): p. 3-33.
5. Shah, A., et al., *Thin-film silicon solar cell technology*. Progress in photovoltaics: Research and applications, 2004. **12** (2-3): p. 113-142.

6. O'regan, B. and M. Gratzel, *A low-cost, high-efficiency solar cell based on dye-sensitized colloidal TiO<sub>2</sub> films.* nature, 1991. **353** (6346): p. 737.
7. Sharma, K., V. Sharma, and S. Sharma, *Dye-sensitized solar cells: fundamentals and current status.* Nanoscale research letters, 2018. **13** (1): p. 381.
8. Irfan, A., *Quantum chemical investigations of electron injection in triphenylamine-dye sensitized TiO<sub>2</sub> used in dye sensitized solar cells.* Materials Chemistry and Physics, 2013. **142** (1): p. 238-247.
9. Tarsang, R., et al., *Τυνιγ τηε ελεστρον δονατινγ αβιλιτψ ιν τηε τριπηνψλαμιν-βασεδ Δ-π-Α αρσητεστυρε φορ ηγηλψ εφφισιεντ δψε-σενσιτζεδ σολαρ σελλς.* Journal of Photochemistry and Photobiology A: Chemistry, 2014. **273** : p. 8-16.
10. Zhang, M., et al., *Design of high-efficiency organic dyes for titania solar cells based on the chromophoric core of cyclopentadithiophene-benzothiadiazole.* Energy & Environmental Science, 2013. **6** (10): p. 2944-2949.
11. Anderson, S., P.N. Taylor, and G.L. Verschoor, *Benzofuran trimers for organic electroluminescence.* Chemistry—A European Journal, 2004. **10** (2): p. 518-527.
12. Park, J.M., et al., *Εφφεστ οφ αδδιτιοναλ πηνοτημαζινε δονορ ανδ τηιοπηνε π-βριδγε ον πηοτοολταις περφορμανςε οφ χυνοξαλινε σορεδ πηοτοσενσιτζερς.* Dyes and Pigments, 2019: p. 107568.
13. Duvva, N., S. Prasanthkumar, and L. Giribabu, *Influence of strong electron donating nature of phenothiazine on A3B-type porphyrin based dye sensitized solar cells.* Solar Energy, 2019. **184** : p. 620-627.
14. Naik, P., et al., *Νεω σαρβαζολε βασεδ μεταλ-φρεε οργανις δψες ωιη Δ-π-Α-π-Α αρσητεστυρε φορ ΔΣΣ"-Σ: Σψντησις, τηεορετιαλ ανδ σελλ περφορμανςε στυδιες.* Solar Energy, 2017. **153** : p. 600-610.
15. Kusumawati, Y., et al., *Combined computational and experimental study of carbazole dyes for iodide- and cobalt-based ZnO DSSCs.* Journal of Photochemistry and Photobiology A: Chemistry, 2017. **341** : p. 69-77.
16. Slimi, A., et al., *Μολεσυλαρ Δεσην οφ Δ-π-ΑΑ Οργανις Δψες Βασεδ ον Τριπηνψλαμιν Δεριατιες ωιη ριους Ανχιλιαρψ Αςεπτορς φορ Ηηη Περφορμανςε ΔΣΣ"-Σ.* Journal of Electronic Materials, 2019: p. 1-11.
17. Manzoor, T., S. Niaz, and A.H. Pandith, *Exploring the effect of different coumarin donors on the optical and photovoltaic properties of azo-bridged push-pull systems: A theoretical approach.* International Journal of Quantum Chemistry, 2019. **119** (18): p. e25979.
18. Carli, S., et al., *A viable surface passivation approach to improve efficiency in cobalt based dye sensitized solar cells.* Polyhedron, 2014. **82** : p. 173-180.
19. Fu, Y., et al., *Theoretical screening and design of SM315-based porphyrin dyes for highly efficient dye-sensitized solar cells with near-IR light harvesting.* Dyes and Pigments, 2018. **155** : p. 292-299.
20. Trabelsi, S., et al., *Intramolecular Path Determination of Active Electrons on Push-Pull Oligocarbazole Dyes-Sensitized Solar Cells.* ChemistryOpen, 2019. **8** (5): p. 580-588.
21. Liu, Y., et al., *Energy Level Control via Molecular Planarization and Its Effect on Interfacial Charge Transfer Processes in Dye-Sensitized Solar Cells.* The Journal of Physical Chemistry C, 2019.
22. ElKhattabi, S., et al., *Theoretical study of the effects of modifying the structures of organic dyes based on N, N-alkylamine on their efficiencies as DSSC sensitizers.* Journal of molecular modeling, 2019. **25** (1): p. 9.
23. Majid, A., et al., *First Principles Study of Dendritic Carbazole Photosensitizer Dyes Modified with Different Conjugation Structures.* ChemistrySelect, 2019. **4** (9): p. 2787-2794.
24. Duan, T., et al., *Triphenylamine-based organic dyes containing a 1, 2, 3-triazole bridge for dye-sensitized solar cells via a 'Click' reaction.* Dyes and Pigments, 2012. **94** (1): p. 28-33.
25. Shi, S., et al., *Εφφεστ οφ Ολιγοτηπηνε π-Βριδγε Λενγτη ον τηε Πηοτοολταις Προπερτιες οφ Δ-Α δπολψμερς Βασεδ ον άρβαζολε ανδ Χυνοξαλινοπορηψιν.* Macromolecules, 2012. **45** (19): p. 7806-7814.
26. Zhang, F., et al., *Triphenylamine-based dyes for dye-sensitized solar cells.* Dyes and Pigments, 2009. **81** (3): p. 224-230.
27. Khazraji, A.C., et al., *Controlling dye (Merocyanine-540) aggregation on nanostructured TiO<sub>2</sub> films. An organized assembly approach for enhancing the efficiency of photosensitization.* The Journal of Physical Chemistry B, 1999. **103** (22): p. 4693-4700.

28. Hara, K., et al., *Effect of additives on the photovoltaic performance of coumarin-dye-sensitized nanocrystalline TiO<sub>2</sub> solar cells*. Langmuir, 2004. **20** (10): p. 4205-4210.
29. Wang, Z.-S., et al., *Photophysical and (photo) electrochemical properties of a coumarin dye*. The Journal of Physical Chemistry B, 2005. **109** (9): p. 3907-3914.
30. Cai, N., et al., *Αν οργανις Δ-π-A δψε φορ ρεσορδ εφφιενγψ σολιδ-στατε σενσιτιζεδ ητεροθυγατιον σολαρ σελλς*. Nano letters, 2011. **11** (4): p. 1452-1456.
31. Li, Y., et al., *Alkali-metal-doped B80 as high-capacity hydrogen storage media*. The Journal of Physical Chemistry C, 2008. **112** (49): p. 19268-19271.
32. Li, G., et al., *Noελ ΤΠΔ-βασεδ οργανις Δ-π-A δψες φορ δψε-σενσιτιζεδ σολαρ σελλς*. Chemical Communications, 2009(16): p. 2201-2203.
33. Li, G., et al., *Efficient structural modification of triphenylamine-based organic dyes for dye-sensitized solar cells*. The Journal of Physical Chemistry C, 2008. **112** (30): p. 11591-11599.
34. Barnsley, J.E., et al., *Benzo [c][1, 2, 5] thiadiazole donor-acceptor dyes: A synthetic, spectroscopic, and computational study*. The Journal of Physical Chemistry A, 2016. **120** (11): p. 1853-1866.
35. Barnsley, J.E., et al., *Flicking the switch on donor-acceptor interactions in hexaazatrinaphthalene dyes: A spectroscopic and computational study*. ChemPhotoChem, 2017. **1** (10): p. 432-441.
36. Hara, K., et al., *Molecular design of coumarin dyes for efficient dye-sensitized solar cells*. The Journal of Physical Chemistry B, 2003. **107** (2): p. 597-606.
37. Zhang, L., J.M. Cole, and C. Dai, *Variation in optoelectronic properties of azo dye-sensitized TiO<sub>2</sub> semiconductor interfaces with different adsorption anchors: carboxylate, sulfonate, hydroxyl and pyridyl groups*. ACS applied materials & interfaces, 2014. **6** (10): p. 7535-7546.
38. Wang, Z.-S., et al., *Hexylthiophene-functionalized carbazole dyes for efficient molecular photovoltaics: tuning of solar-cell performance by structural modification*. Chemistry of Materials, 2008. **20** (12): p. 3993-4003.
39. Sánchez-de-Armas, R., et al., *Direct vs indirect mechanisms for electron injection in dye-sensitized solar cells*. The Journal of Physical Chemistry C, 2011. **115** (22): p. 11293-11301.
40. Duncan, W.R. and O.V. Prezhdo, *Theoretical studies of photoinduced electron transfer in dye-sensitized TiO<sub>2</sub>*. Annu. Rev. Phys. Chem., 2007. **58** : p. 143-184.
41. Nawrocka, A. and S. Krawczyk, *Electronic excited state of alizarin dye adsorbed on TiO<sub>2</sub> nanoparticles: a study by electroabsorption (Stark effect) spectroscopy*. The Journal of Physical Chemistry C, 2008. **112** (27): p. 10233-10241.
42. Homocianu, M., *Solvent effects on the electronic absorption and fluorescence spectra*. Journal of Advanced Research in Physics, 2011. **2** (1).
43. Valentic, N., et al., *Solvent effects on electronic absorption spectra of 3-N-(4-substituted phenyl)-5-carboxy uracils*. Journal of the Serbian Chemical Society, 1999. **64** (3): p. 149-154.
44. Venkatraman, V., Yemene, A.E. & Mello, J. *Prediction of Absorption Spectrum Shifts in Dyes Adsorbed on Titania*. Sci Rep **9**, 16983 (2019)
45. Trivedi, D. and H. Nalwa, *Handbook of organic conductive molecules and polymers*. Wiley, New York, 1997. **2** : p. 505.
46. Venkateswararao, A., et al., *Οργανις δψες σονταινηγ σαρβαζολε ας δονορ ανδ π-λιικερ: οπτισαλ, ελεγτρο-σημισαλ, ανδ πητοολταις προπερτιες*. ACS applied materials & interfaces, 2014. **6** (4): p. 2528-2539.
47. Chen, C.Y., et al., *Multifunctionalized ruthenium-based supersensitizers for highly efficient dye-sensitized solar cells*. Angewandte Chemie International Edition, 2008. **47** (38): p. 7342-7345.
48. Qin, P., et al., *High incident photon-to-current conversion efficiency of p-type dye-sensitized solar cells based on NiO and organic chromophores*. Advanced Materials, 2009. **21** (29): p. 2993-2996.
49. Thongkasee, P., et al., *Carbazole-Dendrimer-Based Donor- -Acceptor Type Organic Dyes for Dye-Sensitized Solar Cells: Effect of the Size of the Carbazole Dendritic Donor*. ACS applied materials & interfaces, 2014. **6** (11): p. 8212-8222.
50. Tan, L.-L., et al., *Novel organic dyes incorporating a carbazole or dendritic 3, 6-diiodocarbazole unit for effcient dye-sensitized solar cells*. Dyes and Pigments, 2014. **100** : p. 269-277.
51. Van Gisbergen, S. J. A., Snijders, J. G., & Baerends, E. J. (1999). Implementation of time-dependent

- density functional response equations. *Computer Physics Communications* , **118** (2-3), 119-138.
- 52. Porezag, D., Frauenheim, T., Köhler, T., Seifert, G., & Kaschner, R. (1995). Construction of tight-binding-like potentials on the basis of density-functional theory: Application to carbon. *Physical Review B* , **51** (19), 12947.
  - 53. Te Velde, G. T., Bickelhaupt, F. M., Baerends, E. J., Fonseca Guerra, C., van Gisbergen, S. J., Snijders, J. G., & Ziegler, T. (2001). Chemistry with ADF. *Journal of Computational Chemistry* ,**22** (9), 931-967.
  - 54. Baerends, E. J., Branchadell, V., & Sodupe, M. (1997). Atomic reference energies for density functional calculations. *Chemical Physics Letters* , **265** (3-5), 481-489.
  - 55. Izmaylov, A. F., Staroverov, V. N., Scuseria, G. E., Davidson, E. R., Stoltz, G., & Cancès, E. (2007). The effective local potential method: Implementation for molecules and relation to approximate optimized effective potential techniques. *The Journal of chemical physics* , **126** (8), 084107.
  - 56. Tarkuc, S., Y.A. Uдум, and L. Toppare, Ταλορηγ της οπτοελεστρονις προπερτιες οφ δονορ-ασεπτορ-δονορ τψη π-σονθυγατεδ πολψμερς ια ωσορπορατινγ διφερεντ ελεστρον-ασεπτορ μοιετιες. *Thin Solid Films*, **2012.520** (7): p. 2960-2965.
  - 57. Kurowska, A., et al., *Effect of donor to acceptor ratio on electrochemical and spectroscopic properties of oligoalkylthiophene 1, 3, 4-oxadiazole derivatives*. *Physical Chemistry Chemical Physics*, **2017. 19** (44): p. 30261-30276.
  - 58. Pathak, S.K., et al., *Columnar self-assembly of star-shaped luminescent oxadiazole and thiadiazole derivatives*. *Journal of Materials Chemistry C*, **2015.3** (12): p. 2940-2952.
  - 59. Chen, F., et al., *Crystal structures, intermolecular interactions and fluorescence properties of a series of symmetrical bi-1, 3, 4-oxadiazole derivatives*. *Journal of Materials Chemistry C*, **2016. 4** (20): p. 4451-4458.
  - 60. Nattestad, A., et al., *Highly efficient photocathodes for dye-sensitized tandem solar cells*. *Nature materials*, **2010. 9** (1): p. 31.
  - 61. Joly, D., et al., *Metal-free organic sensitizers with narrow absorption in the visible for solar cells exceeding 10% efficiency*. *Energy & Environmental Science*, **2015. 8** (7): p. 2010-2018.
  - 62. Cong, J., et al., *Iodine/iodide-free redox shuttles for liquid electrolyte-based dye-sensitized solar cells*. *Energy & Environmental Science*, **2012.5** (11): p. 9180-9194.
  - 63. Yin, N., et al., *Εφφεστ οφ τηε π-σονθυγατον λενγτη ον τηε προπερτιες ανδ πηοτοολταις περφορμανξε οφ A-π-Δ-π-A τψη ολιγοτηιοπηνες ωιη 4, 8-βις (τηιενψλ) βενζο [1, 2-β: 4, 5-β] διτηιοπηνε σορε*. Βειλστειν θουρναλ οφ οργανις ζηεμιστρψ, **2016. 12** (1): π. 1788-1797.
  - 64. Φαηψ, Z.M.E., ετ αλ., *Οπτοελεστρονις προπερτιες οφ τριπηνψλαμινε βασεδ δψες φορ σολαρ σελλ αππισα-τιονις. A ΔΦΤ στυδψ*. *Xuimica Nova*, **2018. 41** (2): p. 129-133.
  - 65. Min, J., et al., *Εφφεστ οφ ολιγοτηιοπηνε π-βριδγε λενγτη ον πηψσιαλ ανδ πηοτοολταις προπερτιες οφ σταρ-σηαπεδ μολεισυλες φορ βυλκ ηετεροθυγατιον σολαρ σελλς*. *Journal of Materials Chemistry A*, **2014. 2** (38): p. 16135-16147.
  - 66. Sutton, J., et al., *Modulation of donor-acceptor distance in a series of carbazole push-pull dyes: A spectroscopic and computational study*. *Molecules*, **2018. 23** (2): p. 421.
  - 67. Lazrak, M., et al. *Τηε σομπυτατιοναλ στυδψ οφ βριδγε εφφεστ ιν Δ-π-A πηοτοοενσιτιε δψες, βασεδ ον τριπηνψλαμινε*. in *IOP Conference Series: Earth and Environmental Science* . 2018. IOP Publishing.
  - 68. Mohammadi, N. and F. Wang, *First-principles study of Carbz-PAHTDDT dye sensitizer and two Carbz-derived dyes for dye sensitized solar cells*. *Journal of molecular modeling*, **2014. 20** (3): p. 2177.
  - 69. Baldenebro-López, J., et al., *Density functional theory (DFT) study of triphenylamine-based dyes for their use as sensitizers in molecular photovoltaics*. *International journal of molecular sciences*, **2012. 13** (4): p. 4418-4432.
  - 70. Bayliss, N.S., *The effect of the electrostatic polarization of the solvent on electronic absorption spectra in solution*. *The Journal of Chemical Physics*, **1950.18** (3): p. 292-296.
  - 71. Ooshika, Y., *Absorption spectra of dyes in solution*. *Journal of the physical society of Japan*, **1954. 9** (4): p. 594-602.
  - 72. McRae, E., *Theory of solvent effects on molecular electronic spectra. Frequency shifts*. *The Journal of Physical Chemistry*, **1957. 61** (5): p. 562-572.

73. Lippert, E., *Dipolmoment und Elektronenstruktur von angeregten Molekülen*. Zeitschrift für Naturforschung A, 1955. **10** (7): p. 541-545.
74. Baur, M.E. and M. Nicol, *Solvent stark effect and spectral shifts*. The Journal of Chemical Physics, 1966. **44** (9): p. 3337-3343.
75. Nicol, M., et al., *Solvent stark effect and spectral shifts. II*. The Journal of Chemical Physics, 1968. **48** (8): p. 3587-3596.
76. Suganya, K. and S. Kabilan, *Substituent and solvent effects on electronic absorption spectra of some N-(substitutedphenyl) benzene sulphonamides*. Spectrochimica Acta Part A: Molecular and Biomolecular Spectroscopy, 2004. **60** (5): p. 1225-1228.
77. Kawski, A., *On the estimation of excited-state dipole moments from solvatochromic shifts of absorption and fluorescence spectra*. Zeitschrift für Naturforschung A, 2002. **57** (5): p. 255-262.
78. Mataga, N., Y. Kaifu, and M. Koizumi, *Solvent effects upon fluorescence spectra and the dipolemoments of excited molecules*. Bulletin of the Chemical Society of Japan, 1956. **29** (4): p. 465-470.
79. Adeoye, M., et al., *Effect of solvents on the electronic absorption spectra of 9, 14 dibenzo (a, c) phenazine and tribenzo (a, c, i) phenazine*. Scientific Research and Essays, 2009. **4** (2): p. 107-111.
80. Galappaththi, K., et al., *Cyanidin-based novel organic sensitizer for efficient dye-sensitized solar cells: DFT/TDDFT study*. International Journal of Photoenergy, Article ID 8564293, **2017**. and Berardo, E., et al., *Modeling excited states in TiO<sub>2</sub> nanoparticles: on the accuracy of a TD-DFT based description*. Journal of chemical theory and computation, 2014. **10** (3): p. 1189-1199
81. Ning, Z., Y. Fu, and H. Tian, *Improvement of dye-sensitized solar cells: what we know and what we need to know*. Energy & Environmental Science, 2010. **3** (9): p. 1170-1181.
82. Mishra, A., M.K. Fischer, and P. Bäuerle, *Metal-free organic dyes for dye-sensitized solar cells: From structure: Property relationships to design rules*. Angewandte Chemie International Edition, 2009. **48** (14): p. 2474-2499.
83. Komaguchi, K., et al., *Electron-transfer reaction of oxygen species on TiO<sub>2</sub> nanoparticles induced by sub-band-gap illumination*. The Journal of Physical Chemistry C, 2009. **114** (2): p. 1240-1245.
84. Sanchez-de-Armas, R., et al., *Electronic structure and optical spectra of catechol on TiO<sub>2</sub> nanoparticles from real time TD-DFT simulations*. Physical Chemistry Chemical Physics, 2011. **13** (4): p. 1506-1514.
85. Mohankumar, V., et al., *Tuning the lifetime from molecular engineering of carbazole donor based metal-free organic dyes for dye sensitized solar cells-A computational approach*. Journal of Molecular Structure, 2019.